Reliability-Oriented Multi-Objective Optimization of Electrical Machines Considering Insulation Thermal Lifetime Prediction

Zhuo Chen, *Student Member, IEEE,* Xiaoyan Huang, *Member, IEEE,* Ang Liu, Ye Ma, Jian Zhang, *Member, IEEE,* Qin Zhang, Rui Wang and Zhaokai Li

***Abstract*—With the trend toward transportation electrification, the power density of electrical machines faces ever-increasing requirement owing to the stringent limit of weight, especially for aerospace applications. Conventionally, the reliability of electrical machines in such safety-critical application is guaranteed by considerable safety margins, i.e., the over-engineering approach, which prevents electrical machines from reaching higher power densities and leads to a design conflict. This paper proposes a reliability-oriented design approach for low-voltage electrical machines by integrating model-based lifetime prediction into a multi-objective optimization process. Accelerated thermal degradation tests are carried out on mainwall insulation and turn insulation, then the thermal degradation model is built to predict the lifetimes, accordingly. Thermal lifetime models are developed at several lifetime percentiles for both continuous duty and variable duty applications. Finally, a feasible reliability-oriented multi-objective optimization platform is established, based on which a study-case electrical machine for aerospace application is designed and optimized. The prototype is manufactured to verify the optimized performances.**

***Index Terms*—Accelerated degradation tests, aerospace application, electrical machines, insulation systems, lifetime modeling, thermal stress**

I. Introduction

The trend toward heavier electrification in transportation applications has been evident worldwide over the past decade [1]. As one of the critical components for the transportation of electrification, electrical machines with high performance including high power/torque density, high reliability and high efficiency have been highlighted [2]. In electric vehicle and high-speed train, the internal combustion engine is being or has been replaced by the high performance electrical machines, demonstrating the technology readiness level of such kind of traction motor [3]-[6]. For aerospace applications, electrical machines with even higher power density and more compact design are desirable as the aircraft is rather sensitive to space and weight [1]. Several long-term research programs in the aerospace sector have stated specific power density targets for electrical machines to be achieved in the coming decades, almost all of which are above 10 kW/kg [7]-[9].

Nowadays, benefit from the ongoing development of various design tools, machine designers are able to perform the multidisciplinary design methodology to achieve satisfactory performance especially in terms of power density [10][11], where multi-domain coupling is inherent and inevitable in such high performance electrical machines. This so-called performance-oriented design method is composed of electromagnetic, mechanical and thermal analysis while the reliability is guaranteed using considerable safety margin. To push the boundary of electrical machines in terms of power density, it is generally achieved by enhancing the electromagnetic load, such as adopting high permeability soft magnetic materials [2][12] and high current density [13], resulting in increased thermal load [14]. The increase in temperature undoubtedly leads to a decrease in reliability, and a well-known example is that the insulation lifetime is halved for every 8℃-10℃ increase in temperature, as stated by the Arrhenius law [14][15]. Due to the safety critical nature of aerospace applications, there is obviously a design conflict between performance and reliability of the electrical machines.

The main factors which constrain the reliability of electrical machines include bearings and insulation system [1]. As the reliability of the bearings can be guaranteed by routine maintenance and replacement [16], the insulation system becomes the primary source of failure [17]. To cope with the reliability issue related to insulation system of electrical machines, high thermal class or thicker insulation is adopted to ensure a sufficient safety margin, known as over-engineering [1][18]. However, such an approach results in a lower slot fill factor and higher thermal resistance, further deteriorating heat dissipation. Moreover, the over-engineering of the electrical machines prevents the insulation material from being used to its full potential, especially for short duty cycle applications such as in the electromechanical actuator (EMA), where the steady-state temperature is far from reaching. As a result, over-engineering enhances the reliability of electrical machines by increasing the use of materials,

Manuscript submitted Jan. 7, 2023; revised Mar. 29, 2023 and May. 7, 2023; accepted Jun. 2, 2023. This work was supported in part by the National Key R&D Program of China (2019YFE0123500), in part by the National Natural Science Foundation of China (51890883) and in part by the Zhejiang Provincial Natural Science Foundation of China (LQ22E070003). *(Corresponding author: Xiaoyan Huang.)*

Zhuo Chen, Xiaoyan Huang, Ang Liu, Ye Ma, Jian Zhang, Qin Zhang and Rui Wang are with Zhejiang Provincial Key Laboratory of Electrical Machine Systems, College of Electrical Engineering, Zhejiang University, Hangzhou 310027, China. (e-mail: z.chen@zju.edu.cn; xiaoyanhuang@zju.edu.cn; a_liu@zju.edu.cn; maye1998@zju.edu.cn; jian_zhang_zju@zju.edu.cn; 21910041@zju.edu.cn; 22010150@zju.edu.cn).

Zhaokai Li is with School of Electrical Engineering and Computer Science, KTH Royal Institute of Technology, Stockholm 11428, Sweden (e-mail: zhaokai@kth.se).

Color versions of one or more of the figures in this article are available online at http://ieeexplore.ieee.orgs

volume and weight, yet with negative effects on power density [1][19] and cost [19]-[22].

Recently, a paradigm shift is taking place in electrical machine design philosophy for aerospace applications, i.e., the reliability-oriented design methodology is emerging as a possible solution [1][19]. The core idea of the reliability-oriented design approach is to replace the traditional empirical-based safety factor with a model-based quantitative reliability analysis, which is then embedded as a reliability constraint in such an emerging design process. Owing to the adoption of physics of failure (PoF) methodologies which enable the precise knowledge and understanding of insulation degradation of electrical machines considering operating conditions featuring the degradation stresses as well as environmental factors [1][19], such quantitative reliability assessment becomes feasible through building appropriate insulation lifetime models. Therefore, the reliability-oriented design method holds the potential to mitigate over-engineering to a substantial extent and further improve the performance of the electrical machines, especially the power density. However, the research to date still focuses on the insulation lifetime modeling and the lifetime assessment of existing electrical machines according to published literature.

In this paper, aiming at dealing with the design conflict between power density and reliability, a reliability-oriented design approach of the low-voltage random-wound electrical machines as well as its possible design procedure is proposed by integrating model-based reliability assessment into performance-oriented design process based on multi-objective optimization. Since the thermal stress is identified as the dominant degradation stress on the insulation system of inverter-fed low-voltage electrical machines, accelerated thermal degradation tests are performed on the mainwall insulation and turn insulation. Consequently, the degradation path is modeled by combining the stochastic process with a PoF-based acceleration model, namely the Arrhenius equation. Lifetime models, based on the Arrhenius life relationship as well as Miner's law, are built through the statistical analysis of lifetimes obtained from insulation thermal degradation model and then employed at the design stage of electrical machines according to the required reliability level, applicable for both continuous duty and variable duty applications. Finally, a feasible reliability-oriented multi-objective optimization platform is built to validate the applicability and effectiveness of proposed method. A study-case electrical machine embedded in an aerospace EMA is designed and optimized based on the platform and a prototype is built to verify the optimized performances.

II. Methodology and Study Assessment

A. Reliability-oriented design scheme

The general flowchart that illustrates the reliability-oriented design scheme of low-voltage electrical machines is given in Fig. 1, and the main implement steps are expressed as follows. First, the optimization objectives and design variables are determined at the initial design stage according to the given design requirements, as are the materials, machine topology and so on. Then, the parametric performance calculation module is built into the multi-optimization process, and the objective and constraint functions are calculated based on its results. Finally, the designs are optimized to generate the Pareto front, from which the optimal design combination is selected. In contrast to the conventional performance-oriented design method, the reliability-oriented design method includes reliability as an optimization goal, enabling the reliability assessment throughout the whole design process. This new methodology is achieved by introducing relevant PoF methodologies into reliability assessment, which allows elaborated lifetime prediction of the insulation system through developing advanced degradation models. Thus, the primary issue is to develop proper lifetime prediction models via the results of reliability tests combined with the knowledge of degradation mechanisms (i.e., using the so-called PoF methodologies).

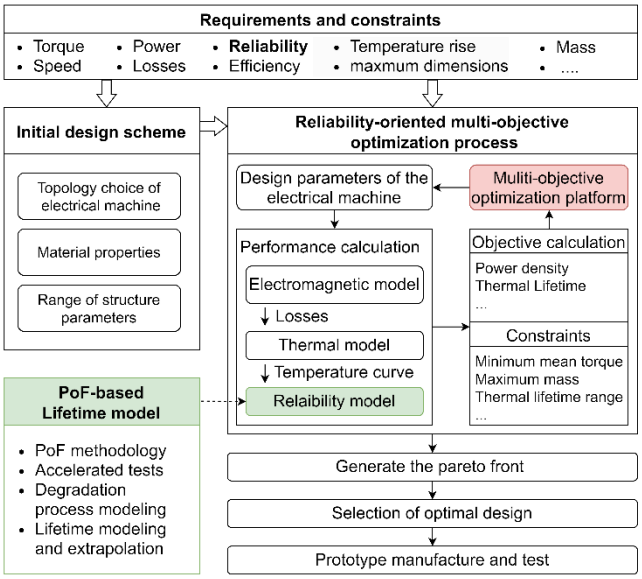

Fig. 1. Flowchart of reliability-oriented design approach for low-voltage electrical machines.

When the electrical machine is operating, the insulation system is exposed to multiple degradation stresses, including thermal, electrical, ambient and mechanical stresses (i.e., the TEAM stresses) [23]. Thus, the near-reality lifetime prediction is realized only through employing proper multi-stress lifetime models, which are often complicated and cumbersome. This is due to the fact that more than one stress simultaneously leads to irreversible degradation of the insulation performance and that there may be interactions between these degradation stresses (including direct and indirect interactions) [23]. In general, it is difficult to quantify individual contribution of simultaneously applied stresses, i.e., direct interaction, in which case simultaneous application of stresses is necessary, leading to complex tests, expensive equipment and even unfeasible accelerated ageing tests. In some specific situations or application contexts, such coupling could be inherently indirect, where these degradation stresses can be applied sequentially or separately, and the superposition principle is

feasible.

Hence, a potential alternative solution is to build single stress lifetime models that can be employed on its own to predict insulation lifetime while possessing the potential to be extended or integrated into multi-stress life model [19]. Such extensions or integrations are feasible under certain conditions that there is indirect or no interaction between or among the degradation stresses, and could be realized, for example, by introducing generalized log-linear models [24] or the multi-stress model with interaction effect [25]. In fact, it is more concise and with greater engineering application potential to evaluate the lifetime of insulation using single stress models individually, based on the common assumption that a certain type of degradation stress dominates during typical operational cycles while others are independent of it or even negligible. This is achieved by identifying the dominant degradation stress as well as its failure mechanism and developing applicable single stress lifetime models relying on the findings of relevant PoF methodology.

B. Discussion on the dominant degradation stress

The hypothesis is made in this paper that thermal stress is the dominant degradation factor, and the discussed lifetime prediction can be achieved using single stress lifetime models. This is put forward based on the inherent characteristics of low-voltage electrical machines for the aerospace application (i.e., partial discharges (PD) free design). Meanwhile, the TEAM stresses to which the machine insulation is exposed should be investigated thoroughly to better frame the lifetime models.

In such safety-critical application, electrical stress is not considered as a primary degradation factor of insulation of low-voltage electrical machines due to the PD-free design. This is because low-voltage random-wound electrical machines commonly adopt organic insulation (Type I insulation), which is sensitive to PD activities and will reach to the end of life shortly once PD activities occur. The effective approach to reasonably confine the PD risk is to ensure that the voltage stressing the insulation system is below the PD inception voltage (PDIV), expressing as follows

$$PDIV > K(t_r) \times a \times V_{DC} \times OF \times EF \tag{1}$$

In (1), V_{DC} is DC link voltage, *OF* is overshooting factor, *EF* is the enhancement factor, $K(t_r)$ is a coefficient depending on the impulse rise time t_r, and a is an empirical coefficient related to the location of the electrical stresses (i.e., $a = 1$ for phase-to-phase insulation, and $a = 0.7$ for phase-to-ground and turn-to-turn insulation). The specific values of *OF*, *EF and* $K(t_r)$ can be found in IEC standard [26] according to the specifications of the variable speed drive (VSD). The PD risks in low-voltage random-wound electrical machines have been carefully investigated in the literature [27]-[29]. Based on these findings, it is possible to state that PD-free machine design for aerospace application is achievable if the VSD reasonably limits the voltage enhancement at machine terminals (e.g., 270V DC link voltage, short connecting cable between machine terminals and converter, and conventional two-level converter using silicon-based insulated gate bipolar transistor (IGBT)).

Generally speaking, the inherent electromagnetic force and external vibration induce mechanical stresses on the machine insulation, causing insulation fatigue, wear, rupture and so on. These weak points accelerate the insulation to failure under the dominant degradation stress. Thus, the mechanical stress is regarded as a secondary degradation factor and can be relieved through impregnation. Meanwhile, the thermomechanical effect is usually ignored, for which it is only applicable to very large machines [30].

The ambient stress, which refers to a series of the environmental factors surrounding the insulation, including humidity, oxygen, etc., is commonly treated as the secondary degradation factor, as well [23]. Each environmental factor can affect the insulation degradation process in different ways yet intends to aggravate the influence of other stresses rather than cause significant degradation on its own [30]. For example, high humidity or low atmospheric pressure reduces the breakdown voltage of air, resulting in lower PDIV and greater PD activities.

C. Accelerated tests

In terms of high-reliability, long-lifetime products for aerospace applications, traditional reliability testing methods usually require a long period of time or a large number of samples, which is difficult for implementation in engineering. Hence, the discussed insulation lifetime prediction is performed using accelerated tests, including accelerated life tests (ALT) and accelerated degradation tests (ADT), where the applied intensity levels of degradation stresses are enhanced to quickly obtain the desired lifetime or performance data while keeping the failure mechanisms the same. ALT is widely used in the evaluation of the insulation lifetime [19], where a collection of lifetimes (namely, time to failure) under enhanced degradation stresses is recorded and employed to extrapolate that under normal service conditions based on a suitable statistical model (i.e., lifetime probability distribution function (PDF) such as normal distribution and Weibull distribution). Instead, in ADT, the diagnostic information under overstress levels (called accelerated degradation data) which describes the degradation path is utilized to build the accelerated degradation model using PoF methodology and consequently determine the lifetimes according to reliability requirements.

In this paper, ADT is chosen to be performed on the stator insulation system due to the advantages over ALT that it is able to give an insight into the degradation process and analyze lifetime earlier before failure [18]. To prepare proper specimens for ADT, precise knowledge of the overall specifications and configurations of the stator insulation system is necessary. The stator insulation system of low-voltage random-wound electrical machines is composed of phase-to-phase, phase-to-ground, and turn-to-turn subsystems, and turn insulation and mainwall insulation are their basic insulation components [14][17][30]. Without loss of generality, turn insulation and mainwall insulation are both considered to be representative of the machine insulation

system on which the ADT is performed in this presented investigation.

III. Modeling of Insulation Thermal Degradation

A. Degradation modeling based on Wiener process

Due to the intrinsic uncertainties of the degradation process, the degradation models based on stochastic process are widely employed [31]. The Wiener-process-based degradation model, which inherits the inherent advantages such as exact physical interpretation and desirable statistical properties [32], reflects great potential to describe the degradation path caused by the accumulation of tiny losses. In this section, the degradation process is modelled as a linear Wiener process.

Let $U(t)$ denote the degradation level of certain insulation diagnostic performance at time t, the degradation process can be described as $\{U(t), t \geq 0\}$. Based on Wiener process, the degradation model is expressed as

$$U(t) = \beta t + \sigma B(t) + U(0) \tag{2}$$

where β is the drift parameter representing the degradation rate, σ is the diffusion parameter, and $B(t)$ is a standard Brown motion process with zero-drift and unit variance which characterizes the stochasticity of the degradation process. It is assumed that the initial value $U(0)$ is zero. Otherwise, the transformation $|U(t) - U(0)|$ can be made to satisfy this assumption.

In order to obtain the degradation process under working stress, the relations between model parameters and accelerated stresses should be derived. As is well known that the premise of ADT is that the failure mechanism remains the same under either normal stress or accelerated stress [31], the further assumption is made that the model parameters, i.e., the drift parameter β and the diffusion parameters σ, are stress-related. For the sake of simplicity, the drift parameter β_j and diffusion parameters σ_j remain constants under certain degradation stress T_j. The most popular approach is using acceleration models based on PoF. Since thermal stress is the dominant degradation factor, where the thermal degradation mechanism of Type I insulation is internal chemical reaction [15], the Arrhenius model which reflects the temperature-dependent chemical reaction rate is chosen and provided as follows:

$$\kappa = A e^{-\frac{E_a}{RT}} \tag{3}$$

where κ denotes the parameter related to reaction rate, T denotes the degradation stress, i.e., temperature expressed in Kelvin, A denotes the constant associated to the ADT method, failure mechanism and other factors, E_a denotes activation energy, R represents the Boltzmann constant and $R = 8.6171 \times 10^{-5} eV/K$. Thus, by linearizing (3), the drift parameter β_j and the diffusion parameter σ_j at the degradation stress level T_j can be obtained as

$$\begin{cases} \ln \beta_j = \ln A_\beta - \gamma_\beta / T_j \\ \ln \sigma_j^2 = \ln A_{\sigma^2} - \gamma_{\sigma^2} / T_j \end{cases} \tag{4}$$

where A_β, A_{σ^2}, γ_β and γ_{σ^2} are undetermined coefficients.

Based on the accelerated degradation data, the drift parameter β_j and the diffusion parameter σ_j can be estimated. It is assumed that the specimens are exposed to constant accelerated degradation stresses in this study. Under the *j-th* degradation stress level T_j, the value of certain insulation diagnostic performance U_{jkl} is measured at corresponding time t_{jkl}, where k represents the k-th sample, l represents the l-th measurement, n_j denotes the total number of degradation stress levels, n_k represents the total number of samples, n_l represents the total number of measurements per sample, $j = 1, 2, \ldots, n_j$, $k = 1, 2, \ldots, n_k$ and $l = 1, 2, \ldots, n_l$. The degradation increment ΔU_{jkl} is defined as $\Delta U_{jkl} = U_{jkl} - U_{jk(l-1)}$ during the corresponding time interval $\Delta t_{jkl} = t_{jkl} - t_{jk(l-1)}$. According to the properties of Wiener process, the increments follows a normal distribution, expressed as $\Delta U_{jkl} \sim N(\beta_j \Delta t_{jkl}, \sigma_j^2 \Delta t_{jkl})$. Thus, β_j and σ_j^2 can be estimated using maximum likelihood estimation(MLE) method and the log-likelihood function is constructed as

$$\ln \mathcal{L}_j(\Delta U_{jkl}; \beta_j, \sigma_j^2) = \sum_{k=1}^{n_k} \sum_{l=1}^{nl} \left(-\frac{1}{2} \ln(2\pi\sigma_j^2 \Delta t_{jkl}) - \frac{(\Delta U_{jkl} - \beta_j \Delta t_{jkl})^2}{2\sigma_j^2 \Delta t_{jkl}} \right) \tag{5}$$

By substituting estimated pairs $\left(\hat{\beta}_j, \hat{\sigma}_j^2\right)$ into (4), these four parameters A_β, A_{σ^2}, γ_β and γ_{σ^2} can be determined and used in further lifetime prediction.

B. Test campaign and data analysis

To investigate the influence of thermal stress on mainwall insulation and turn insulation, two kinds of typical and commonly used specimens are chosen for the ADTs. For mainwall insulation specimens (i.e., slot liner), the 0.25-mm-thick polyimide (PI) films whose thermal class is above 200℃ are selected, as shown in Fig. 2(a). A total number of 45 specimens were prepared from the same batch of product and divided randomly into three groups for the ADT. To ensure that the failure mechanism keeps consistent under accelerated degradation stress and working stress, three constant accelerated stress levels, with an interval of 10℃ [23][33], were selected as T_1 = 290℃, T_2 = 300℃ and T_3 = 310℃. The specimens were aged at these temperatures in a ventilated oven shown in Fig. 2(c), separately. After each thermal exposure cycle, the breakdown voltages of the specimens, which represent the electric strength, were tested in air at room temperature using direct voltage. This is a destructive test following the procedures indicated in the technical standard [34]. Each specimen was measured only once and the test lasted until all specimens have been measured. The initial values of breakdown voltage U_{ini} were measured before ADT.

For turn insulation specimens, random wound coils, whose thermal lifetimes are the most conservative among several kinds of turn insulation specimens (i.e., motorettes, twisted pairs and coils) [14], are selected, shown in Fig. 2(b). Three sets of a total of twelve random wound coils have been manufactured using Class 200, Grade 2, 0.45-mm diameter round copper wire with a dual coating (i.e., a modified polyester underlying coating with a polyamide-imide superimposed coating) and impregnated with epoxy resin. Similarly, each set of specimens is thermally degraded in the ventilated oven at constant temperatures, i.e., T_1 = 200℃, T_2 =

210℃ and T_3 = 220℃. The dielectric dissipation factor (i.e., tanδ) between strands, which directly indicates the thermally degradation level of turn-to-turn insulation [30][35], is measured using a Megger IDAX300 after each thermal exposure cycle.

(a) (b) (c)

Fig. 2. Thermally accelerated degradation tests performed on mainwall insulation and turn insulation. (a) Polyimide film specimens. (b) Random-wound coil specimens. (c) The ventilated oven.

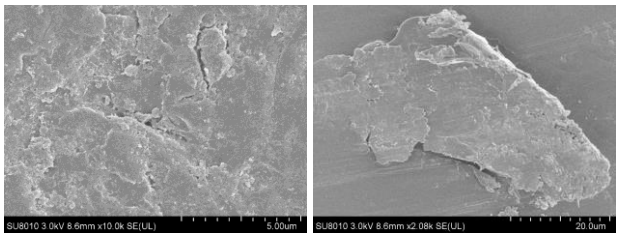

Fig. 3. The surface morphology of thermally aged specimens observed by a field emission scanning electron microscope.

As shown in Fig. 2(a), the color of the mainwall insulation specimen darkens after ADT, revealing the degradation caused by thermal stress. Furthermore, the surface morphology of thermally aged mainwall insulation specimens were investigated using a field emission scanning electron microscope, illustrated in Fig. 3. Local cracks and delaminations were observed on certain specimens.

The remaining breakdown voltages of mainwall insulation specimens under each stress level are depicted in Fig. 4(a). In general, the dielectric performance of the mainwall insulation specimens decline monotonically under accelerated thermal stress. The performance decreases faster with the increase of the thermal stress level. Similarly, the dielectric dissipation factors of turn insulation specimens are given as a function of the degradation time in Fig. 4(b). The results show monotonically increasing trends, with respect to both the degradation time and increasing temperatures. The degradation paths under each accelerated stress level are be predicted using the proposed Wiener-process-based degradation model with estimated parameters $\left(\hat{\beta}_j, \hat{\sigma}_j^2\right)$, shown in Fig. 5. It is apparent that the estimated degradation paths generally agree with the actual ones. The average estimation errors of the Wiener-process-based degradation model are within 6.3% and 10.5% for the diagnostic performances of mainwall insulation and turn insulation specimens, respectively. Considering the measurement errors and random factors, the results implies that the proposed degradation model can reasonably predict the insulation degradation paths.

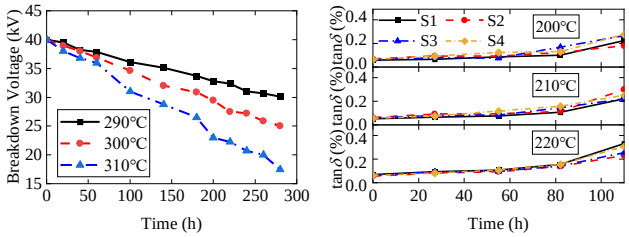

(a) (b)

Fig. 4. Diagnostic performances of mainwall insulation and turn insulation specimens under three accelerated stress levels. (a) The remaining breakdown voltages. (b) The dielectric dissipation factors (i.e., tanδ).

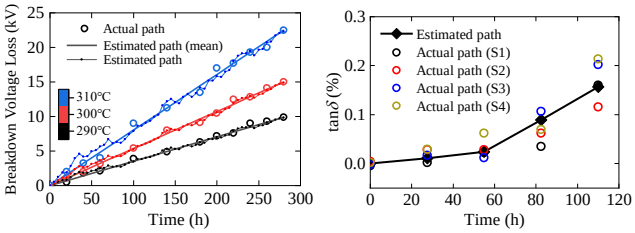

(a) (b)

Fig. 5. The actual and estimated degradation paths of the specimens under accelerated stress levels. (a) Cumulative loss of breakdown voltage of mainwall insulation specimens. (b) Increments of the dissipation factor of turn insulation specimens at 200℃.

IV. Lifetime Model

In the case of PD-free low-voltage motors for aerospace applications where thermal stress is the dominant degradation stress, it is feasible to derive the lifetime model to predict the remaining useful life of insulation based on the proposed degradation model as well as the understanding of the degradation process. These lifetime models are built at several certain lifetime percentiles according to the reliability requirements of the applications, considering various duty types of the motors. They may therefore be utilized as analysis tools for safety checks of existing electrical machines or as design tools embedded in reliability-oriented design for safety-critical applications.

The first hitting time (FHT) is used to define the end of life when the degradation path $\{U(t), t \geq 0\}$ exceeds the predefined failure threshold ω_f for the first time. The lifetime L is defined as

$$L = \inf\{t \mid U(t) \geq \omega_f, t \geq 0\} \tag{6}$$

The FHT of Wiener process follows an inverse Gaussian distribution, whose PDF $f_L(t)$ and reliability function $R_L(t)$ are given by [32][36]

$$f_L(t) = \frac{\omega_f}{\sqrt{2\pi\sigma^2 t^3}} \exp\left(-\frac{(\omega_f - \beta t)^2}{2\sigma^2 t}\right) \tag{7}$$

$$R_L(t) = P\left(U(t) \leq \omega_f\right) = \Phi\left(\frac{\omega_f - \beta t}{\sigma\sqrt{t}}\right) - \exp\left(-\frac{2\beta\omega_f}{\sigma^2}\right)\Phi\left(-\frac{\omega_f + \beta t}{\sigma\sqrt{t}}\right) \tag{8}$$

where $\Phi(\bullet)$ represents the cumulative distribution function of the standard normal distribution.

It is necessary to state how to determine the failure threshold. Concentrating on the main insulation made from organic material (i.e., Type I insulation), the maximum allowable value of the phase-to-ground voltage $U_{\max\ \text{p-e}}$, calculated by (9) guarantees reliable operation of the machines fed by pulse width modulation (PWM) inverter, beyond which the insulation breaks down in a short period of time [38]

$$U_{\max\ \text{p-e}} = 1000V + (2 \times U_N \times TVF) \tag{9}$$

Here, U_N is the rated voltage of the machine, *TVF* is the test voltage factor depending on the impulse voltage insulation class (IVIC). The value of *TVF* ranges from 0.7 to 1.7 according to IVIC [26]. Thus, the failure threshold is characterized by the cumulative degradation increment of breakdown voltages, calculated as

$$\omega_f = U_{\text{ini}} - k \cdot U_{\max\ \text{p-e}} \tag{10}$$

where k is an empirical coefficient depending on the test method of the breakdown voltage. In particular, k is recommended to be 1.7 in [30] and [39] if DC voltage was used in such test, exactly as the preformed ADT. For example, supposing a inverter-fed electrical machine is rated for 200V whose insulation system has been qualified for extreme impulse stress (i.e., IVIC D), the $U_{\max\ \text{p-e}}$ is obtained to be 1.68 kV using (9) and then ω_f is 37.14 kV, where *TVF*= 1.7 at IVIC D and U_{ini} = 40 kV. As for turn insulation, there are no published papers, technical documents, or standards that specify the failure threshold of the dielectric dissipation factor for low-voltage random-wound electrical machines. Referring to some related acceptance criteria in literatures [30][42]-[44] and considering the thermal endurance class of the turn insulation specimens, the failure thresholds is set to be tanδ = 20% in this study.

The expectation L, namely the mean time to failure (MTTF), is calculated from

$$E(L) = MTTF = \int_0^\infty t f(t) dt = \frac{\omega_f}{\beta} = \frac{\omega_f}{A_\beta} \exp\left(\frac{\gamma_\beta}{T_j}\right) \tag{11}$$

Furthermore, given desired reliability α, i.e., $\alpha = R_L(t_\alpha)$, the lifetime t_α is found from $t_\alpha = R_L^{-1}(\alpha)$, where $R_L^{-1}(\bullet)$ denotes the inverse function of the reliability function given by (8). The lifetime percentile $B\rho$ ($\rho = 100(1-\alpha)$) is also provided by the definition of t_α, which indicates a predetermined percentage of population will reach the end of life at t_α. For instance, supposing that α is set to be 0.99, $t_{0.99}$ is referred to as *B*1 lifetime when 1 percent of the samples while have failed. So is *B*50 lifetime $t_{0.5}$, i.e., the median time to failure depicting the central tendency of the data with high skewness [37]. *B*50 lifetime is almost equal to MTTF when the skewness is small (i.e., $\omega_f \beta / \sigma^2 > 2$ in this study which is always satisfied in the subsequent evaluation).

However, since the reliability function is not entirely composed of elementary functions, numerical computation method should be applied to obtain t_α, which is cumbersome and time-consuming. A graphical data analysis method, i.e., Arrhenius plot, is used to extrapolate the lifetime-temperature relationship, supposing that the Arrhenius life relationship is valid at the tested temperatures [15][18][19]. The reliability functions with the locations designated by the corresponding temperatures are imported on Arrhenius plot to determine the lifetime-temperature curves at several lifetime percentiles. Then, each curve is drawn by interpolating the "lifetime dots" at certain temperatures. Fig. 6 illustrates an example of the Arrhenius plot where the lifetime percentiles *B*1 and *B*50 are supposed. Furthermore, it is worthy to stress that any other lifetime percentiles could be selected, which relies on the reliability specification of the practical application.

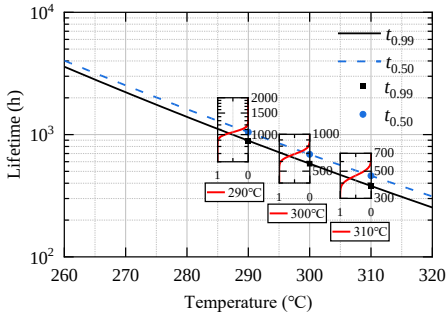

Fig. 6. Arrhenius plots of mainwall insulation at *B*1 and *B*50 lifetime percentiles.

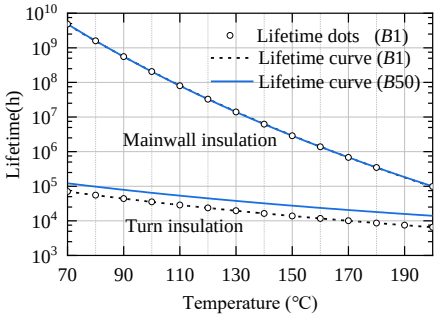

Fig. 7. Arrhenius lifetime-temperature relationships of both mainwall insulation and turn insulation within operating temperature range of the electrical machine.

The Arrhenius-Dakin's equation [15][19][40] is introduced to characterize the lifetime-temperature curves (or thermal endurance curves) in the Arrhenius plot, given by

$$LF_{B\rho}(T_j) = A_{B\rho} \exp\left(\frac{R_{B\rho}}{T_j}\right) \tag{12}$$

where $LF_{B\rho}$ is the lifetime at a certain lifetime percentile, $A_{B\rho}$ and $R_{B\rho}$ are undetermined coefficients related to the insulation material property and ADT method, graphically obtained by fitting the "lifetime dots". For the sake of completeness, the Arrhenius plot with a more extensive scale of horizontal axis covering the operating temperature range of electrical machines is reported in Fig. 7 for *B*1 and *B*50 lifetime percentiles. Meanwhile, the results indicate that turn insulation is the weakest part of stator insulation system of low-voltage random-wound electrical machines, whose lifetime represents the bottleneck in terms of reliability and should be optimized in the reliability-oriented design.

As for electrical machines working in continuous duty type applications which features almost constant steady-state temperatures, the lifetime of insulation under single thermal stress can be predicted at ease by substituting the constant steady-state temperature in (12) in accordance with the

reliability specification. The temperature can be obtained from experiments or thermal models.

In aerospace applications, most of the electrical machines work at variable duty, where the operation time is not sufficient to reach the thermal equilibrium and a profile is required to depicts the temperature variation tendency. The lifetime prediction model at variable duty (i.e., time-variable temperature) can be derived based on the cumulative damage law of Miner [41]. Supposing a general temperature profile $T_j(t)$ within the timespan Δt_{cycle}, the transient temperature during an infinitesimal time interval dt can be regarded as a constant. The infinitesimal element fraction $dLoL_{B\rho}$ which represents the loss of life of insulation in this interval dt is expressed as

$$dLoL_{B\rho} = \frac{dt}{LF_{B\rho}(T_j(t))} \tag{13}$$

The loss of life $LoL_{\Delta t_{cycle}}$ is calculated by the integral of $dLoL_{B\rho}$ within each thermal cycle Δt_{cycle} at a predetermined lifetime percentile, expressed as follows

$$LoL_{\Delta t_{cycle-B\rho}} = \int_0^{\Delta t_{cycle}} dLoL_{B\rho} = \int_0^{\Delta t_{cycle}} \frac{1}{A_{B\rho}} \exp\left(-\frac{R_{B\rho}}{T_j(t)}\right) dt \tag{14}$$

Then, the total lifetime $LF_{Bd\text{-}B\rho}$ is determined by taking into account the number of the cyclical thermal stress cycles the insulation experienced, i.e., the theoretical number of cycles to failure $N_{B\rho}$, calculated as follows.

$$LF_{vd-B\rho} = \frac{1}{LoL_{\Delta t_{cycle-B\rho}}} \cdot \Delta t_{cycle} = N_{B\rho} \cdot \Delta t_{cycle} \tag{15}$$

V. Reliability-Oriented Multi-Objective Optimization

A. Study case

To demonstrate the reliability-oriented methodology and give a practical example of lifetime prediction, a permanent-magnet synchronous motor (PMSM) is designed for the flap EMA of a certain type of aircraft. The main specifications and design requirements of the study-case PMSM as well as its driving system are provided in TABLE I. As this study-case PMSM is fed by a conventional two-level voltage source inverter (VSI) based on Si-IGBT, a short connecting cable (no more than 0.5 m in this case) between PMSM and VSI is considered for the purpose of reducing the enhancement of machine terminal voltage caused by transmission line reflections [26] and realizing the compactness of the EMA level. It is evident that the premise of the proposed lifetime models that thermal stress is the dominant degradation factor is satisfied as it is a PD-free electric drive system according to TABLE I.

The mission profiles of the EMA and the PMSM are given in Fig. 8, which illustrate the target to be achieved in the worst case that the EMA fulfills a full flap extension, holding and retraction cycle at motor peak torque in a time period of 18 s. Several cycles should be performed without any cooling time for safety considerations [14] and four continuous cycles are required in this study.

TABLE I

THE DESIGN REQUIREMENTS OF THE STUDY-CASE PMSM

Parameter	Value	Unit
Rated speed	3000	rpm
Peak torque	>22.5	N·m
DC link voltage	270	V
Switching frequency	8	kHz
Lifetime (MTTF)	$\geqslant 2.5\times10^4$	h
Power density	$\geqslant$1.5	kW/kg
Cooling method	Natural cooling	

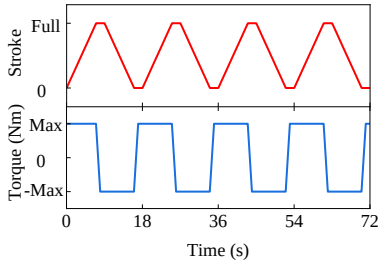

Fig. 8. Mission profiles of the EMA and the study-case PMSM.

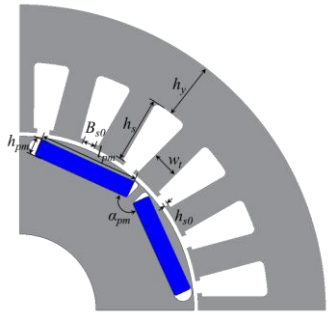

Fig. 9. The topology and parametric model of the study-case PMSM.

B. Multi-objective optimization

Fig. 9 illustrates the topology and parametric model of the study-case PMSM, which employs a set of three-phase double-layer winding and interior PM configuration. A total of 9 design parameters are chosen as optimization variables, whose initial values and optimization ranges are summarized in TABLE II. As the applicability of the proposed lifetime model in this application scenario has been clarified, the optimization objectives are to maximize the power density $f_{SP}(x_i)$ and the insulation thermal lifetime $f_{LF}(x_i)$ of the PMSM. The power density is defined as the ratio of output power to effective mass, expressed as

$$f_{SP}(x_i) = \frac{T_{avg}\Omega}{m_a} \tag{16}$$

where T_{avg} is the average output torque, Ω is mechanical angular velocity and m_a is effective mass (only stator and rotor are included) and x_i represents the optimization variable shown in TABLE II. Since the reliability requirement of this short-duty aerospace PMSM, i.e., insulation thermal lifetime, is given by MTTF in this study, the total lifetime $f_{LF}(x_i)$ is predicted using the variable-duty lifetime model and represented by the smaller one between mainwall insulation and turn insulation. Each design $\mathbf{y} = \left(f_{SP}(x_i), f_{LF}(x_i)\right)$ gives

a point in the 2-dimensional objective space.

In this multi-objective optimization, the following constraints should be satisfied

$$\begin{cases} V_{PM} \le 2\times10^{-6}\ \mathrm{m}^3 \\ T_{\mathrm{avg}} \ge 22.5\ \mathrm{N\cdot m} \\ x_i^L \le x_i \le x_i^U \quad i=1,2,...,9 \end{cases} \tag{17}$$

where V_{PM} is the PM volume of one pole-pair, x_i^U and x_i^L are upper and lower limits of corresponding variable.

TABLE II

INITIAL VALUES AND OPTIMIZATION RANGES OF OPTIMIZATION VARIABLES.

Parameter	Definition	Initial value	Range
h_y (mm)	Thickness of stator yoke	13.3	10.6-16.0
h_s (mm)	Depth of slot	13.5	10.8-16.2
w_t (mm)	Width of stator teeth	4.6	3.7-5.5
B_{s0} (mm)	Slot opening	2.9	2.3-3.5
l_{pm} (mm)	Magnet length	18.9	15.1-22.7
h_{pm} (mm)	Magnet thickness	4.2	3.4-5.0
α_{pm} (°)	Angle between V-shape PMs	134.7	107.8-161.6
L_{acl} (mm)	Active stack length	62.1	49.7-74.5
J_s (A/mm^2)	Slot current density	13.1	10.5 -15.7

Based on PlatEMO [45] and the framework given in Fig. 1, the reliability-oriented multi-optimization platform is established in Matlab environment. The parametric electromagnetic model is built in FEMM, an open-source FEM software, where the electromagnetic performances, including torque and losses, are calculated and delivered to the parametric thermal model built with Motor-CAD. Based on the thermal results, the lifetimes of the designs are predicted using the proposed lifetime model.

The parametric thermal model is based on a 3-dimensional lumped parameter thermal network (LPTN). Most of the parameters in the LPTN can be calculated with considerable accuracy, such as thermal resistances and capacitances, provided that the machine geometry and material properties are well-defined [46]. However, some critical parameters related to manufacturing or other uncertainties must be fine-tuned to ensure the considerable prediction accuracy. The following critical model parameters are chosen to be fine-tuned, which are listed as follows:

1) interface gap between stator lamination and housing $g_{s\text{-}h}$;
2) emissivity of housing ε_h;
3) external natural convection heat transfer coefficients for fin base h_{r1}, fin side h_{r2} and fin tips h_{r3};
4) gap between slot liner and stator lamination $g_{s\text{-}l}$ and material in the gap;
5) the minimum separation between conductors g_{con};
6) thermal conductivity of impregnation epoxy k_{epy};
7) impregnation goodness coefficient c_{ipg}.

The gaps $g_{s\text{-}h}$ and $g_{s\text{-}s}$ account for the uncertain thermal contact resistances the between contacting surfaces of stator lamination and housing, as well as stator lamination and slot liner, respectively. The parameters g_{con}, h_{epy} and c_{ipg} incorporate the uncertainty in the winding from manufacturing which affect the heat flow by conduction. The parameter ε_h, which determines the heat dissipation due to external radiation, needs to be tuned to consider housing surface manufacturing. The parameter h_r accounts for the variables influencing heat transfer by convection, including the housing surface geometry, the motion and property of air.

TABLE III reports the determined critical thermal parameters which have been experimentally fine-tuned. To verify the thermal model, the thermal experiment with a variable load duty cycle has been carried out. Fig. 10 presents the measured and predicted winding temperature curves of the case-study PMSM, where the predicted temperature refers to the detected hot spot temperature of the winding in the experiment. Good agreement between experimental and predicted temperature curves is observed and validates the thermal model.

One of the most popular multi-objective evolutionary optimization algorithms, NSGA-II, combining the fast non-dominated sorting, elitist and crowding distance, is adopted in this study. The utilization of a parameterless niching operator in NSGA-II confers benefits to the algorithm, as it is not highly sensitive to the parameter settings [47]. Thus, the default parameter setting outlined in TABLE IV is applied during optimization in PlatEMO [45]. This approach ensures that the algorithm operates optimally without the need for extensive parameter tuning. The optimization process is carried out using a population size of 20 and 300 generations.

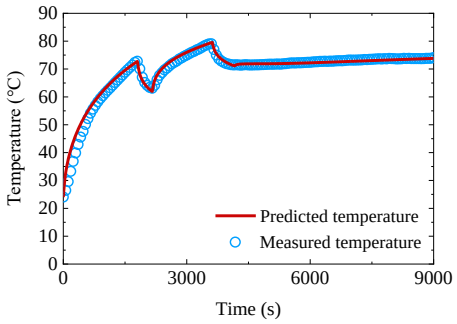

Fig. 10. Measured and predicted winding temperature curves of the case-study PMSM.

TABLE III

THE TUNED CRITICAL PARAMETERS OF THE THERMAL MODEL

Parameter	Value
$g_{s\text{-}h}$ (mm)	0.08
ε_h	0.1
h_{r1} (W/m^2·K)	5.81
h_{r2} (W/m^2·K)	5.68
h_{r3} (W/m^2·K)	6.04
$g_{s\text{-}s}$ (mm)	0.05/epoxy
g_{con} (mm)	0.05
h_{epy} (W/m·K)	1.25
c_{ipg}	0.8

TABLE IV

PARAMETER SETTING OF NSGA-II

Parameter	value	Parameter	value
Population	20	Generation	300
Probability of crossover	1	The distribution index of simulated binary crossover	20
The expectation of the	1	The distribution index of	20

number of mutated variables | polynomial mutation

The modified generational distance (denoted by GD+) is introduced as the convergence indicator in the multi-objective optimization. Given a solution set $S_m = \{\boldsymbol{y}_{m1}, \boldsymbol{y}_{m2}, ..., \boldsymbol{y}_{mN_s}\}$ consisting of N_s normalized designs $\boldsymbol{y}_{mi} \in [0,1]^2$ of m-th generation, and a reference set $R = \{\boldsymbol{y}_1^*, \boldsymbol{y}_2^*, ..., \boldsymbol{y}_{N_r}^*\}$ with N_r normalized non-dominated solutions $\boldsymbol{y}_i^* \in [0,1]^2$, the convergence indicator GD$^+$ is defined as follows [48]:

$$GD^+(S_m) = \frac{1}{N_m}\left(\sum_{i=1}^{N_m}\left(\sqrt{\left(\sum_{k=1}^{2}\max\left\{\boldsymbol{y}_{mi,k} - \boldsymbol{y}_{j,k}^*, 0\right\}\right)^2}\right)^p\right)^{\frac{1}{p}} \quad (18)$$

where $\boldsymbol{y}_{j,k}^*$, $j = \{1, ..., N_r\}$ is the closest solution to $\boldsymbol{y}_{mi,k}$ in the reference set, p is an integer set to be 1 in this study, and $\boldsymbol{y}_{j,k}^*$ with k = 1, 2 indicate the normalized power density and lifetime of design $\boldsymbol{y}_j^*$, respectively. The reference set is uniformly sampled from the approximate Pareto front, which is generated using a Gaussian process regression (GPR) to approximate the unknown, theoretical Pareto front [49].

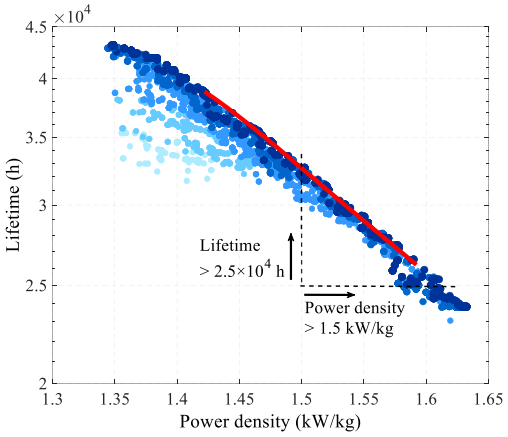

Fig. 11. The optimization space (blue dots) and the approximate Pareto front (red continuous line) with respect to machine power density and insulation thermal lifetime.

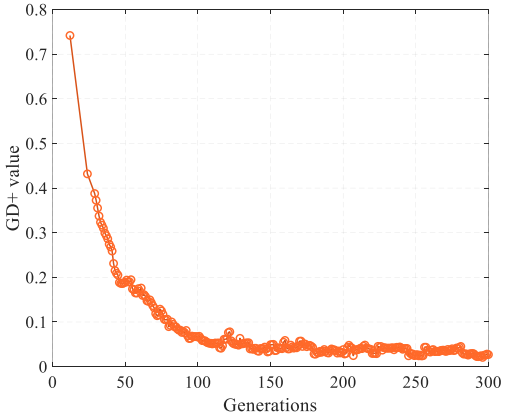

Fig. 12. The modified generational distance GD+ as a function of the generations.

Fig. 11 illustrates all of the 6,000 potential designs in the optimization space and the approximate Pareto front. It is obvious that the nature of conflict between the two optimization objectives does exist, and the tradeoff between them is necessary in the design process. After 300 generations, the GD$^+$ values gradually decreased to under 0.05, indicating the convergence of the optimization was reached, as shown in Fig. 12.

VI. Comparison and Verification

Based on the Pareto front, it is possible to achieve the tradeoff between power density and reliability at the level of Pareto optimality at the early design stage of high-performance electrical machines. The case study presented in this paper outlines the design requirements of power density and insulation thermal lifetime (MTTF), which are specified as being no less than 1.5 kW/kg and $2.5 \cdot 10^4$h, respectively, and can be found in TABLE I. Based on these requirements, the optimal design was selected using a tradeoff criterion that involved identifying the design point on the Pareto front with the longest lifetime when the power density requirement was reached. This resulted in a design with a predicted power density of 1.5 kW/kg and an insulation thermal lifetime of $3.271 \cdot 10^4$h. The optimal combination of design parameters is listed in TABLE V, while the main dimensions and materials of the study-case PMSM are given in TABLE VI. It is worth noting that a margin was included in the selection of the insulation thermal life to account for the accuracy of the thermal model.

The predicted average torque, weight and power density are 24.03Nm, 4.75kg and 1.59kW/kg for the initial design, and 24.78Nm, 5.19kg and 1.50kW/kg for optimal design, respectively. In terms of lifetime, it is well improved comparing with the initial design, from $1.060 \cdot 10^4$h to $3.271 \cdot 10^4$h.

TABLE V

Selected Optimal Values of Design Parameters

Parameter	Value	Parameter	Value
h_y (mm)	11.2	h_{pm} (mm)	3.5
h_s (mm)	12.9	α_{pm} (°)	140
w_t (mm)	5.5	L_{act} (mm)	68
B_{s0} (mm)	2.5	J_s (A/mm^2)	12.33
l_{pm} (mm)	20		

TABLE VI

Main Specification of the Study-Case PMSM

Parameter	Value
Number of slots/pole pairs	24/2
Peak torque (N·m)	25
Stator outer diameter (mm)	120
Thickness of tooth-tip (mm)	0.85
Air-gap length (mm)	0.8
Rotor inner diameter (mm)	30
Number of turns per slot	24
Number of parallel branches	4
Slot fill factor (Copper)	Around 35%
Stator/rotor core material	20 JNEH1200
PM material	N42EH
Mainwall insulation (slot liner)	Polyimide film 6050 (0.25 mm)
Magnet wire	Polyester overcoated with polyamide-imide enamelled round copper wire,

Class 200, Grade 2, 0.45 mm-diameter

To validate the proposed methodology, a prototype of the study-case PMSM was manufactured based on the optimization result. The prototype's stator insulation configuration is nearly identical to that used in the performed ADT. Fig. 13(a) shows stator and rotor of the prototype, Fig. 13(b) shows the test bench. Fig. 14 depicts the magnetic flux density of the prototype at no load and peak load conditions. Fig. 15(a) compares the no-load line-to-line back-EMF from experiment and FEM simulation. Fig. 15(b) shows the simulated torque waveform at peak load condition. The torque ripple is 8.9%, complying with the general design requirements. The torque-current characteristic is calculated using FEM under the $i_d = 0$ control method and experimentally validated. The comparison between measured and FEM calculated curves is shown in Fig. 15(c), which shows a good agreement. The torque constants of the prototype calculated from measured and FEM data are 0.205 N·m/A and 0.197 N·m/A, respectively, where a maximum mismatch of 4.1% is observed. The prototype is characterized by an effective mass of 5.13 kg and achieves a power density of 1.57 kW/kg at 25.63 N·m and 3000 rpm in the experiment, meeting the design target for power density.

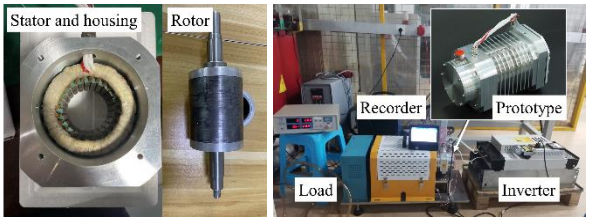

(a) (b)

Fig. 13. The prototype and test bench. (a) Stator, housing and rotor. (b) Test bench.

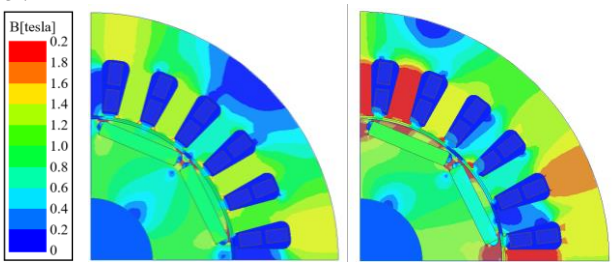

(a) (b)

Fig. 14. Magnetic flux density distribution of the prototype. (a) No load condition. (b) Peak load condition.

To validate the reliability of the prototype (i.e., the insulation thermal lifetime in this study), temperature curves have also been recorded directly from the experiment using pre-embedded thermal resistors (i.e., Pt100) in the prototype, shown in Fig. 16. For experimental simplicity, the mission profile of the PMSM is simplified to consist of covering a full load in 6 s, followed by 60 s load holding and then unloading. The highest temperature curve in Fig. 16, which characterizes the temperature of a winding hot-spot, is selected for conservative assessments, and the curve is raised to start at 70 ℃ to consider the worst scenario (i.e., ambient temperature) in aerospace applications [19]. Based on the proposed lifetime model, the loss of life of the turn insulation within such a thermal cycle is obtained, depicted in Fig. 17. The number of cycles to failure $N_{B\rho}$ as well as lifetime $LF_{vd\text{-}B\rho}$ corresponding to the given EMA mission profile are summarized in TABLE VII. For the sake of completeness, the lifetimes are also evaluated using the continuous duty model by replacing in (12) the highest point in the temperature curve (i.e., 170.5 ℃), also summarized in TABLE VII. It is clear that the lifetime predicted through the continuous duty model is far more conservative for replacing the steady-state temperature with the peak temperature, which confirms the necessity of building the lifetime models for both continuous and variable duty electrical machines. Taking N_{B50} as an example, it can be interpreted as meaning that the PMSM will face a 50% failure probability after completing $5.360 \cdot 10^5$ EMA missions and the failure only results from the breakdown of turn insulation caused by thermal stress. The corresponding MTTF of turn-to-turn insulation is $3.230 \cdot 10^4$ h, which is close to the optimized lifetime and satisfies the design requirement in terms of reliability.

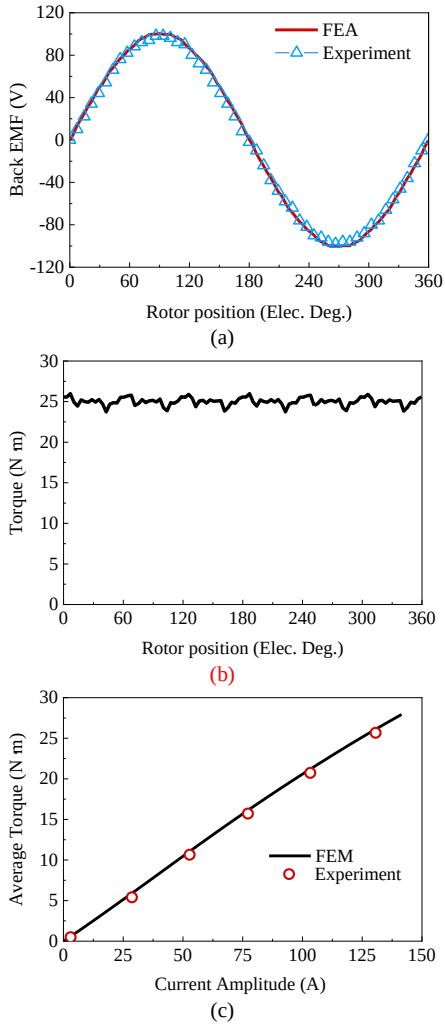

Fig. 15. FEM and experimental results of the prototype. (a) The line-to-line back-EMF. (b) The simulated torque waveform at peak load condition. (c)The average torque versus current amplitude.

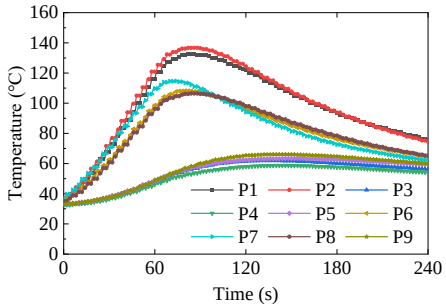

Fig. 16. The experimental temperature curves at different locations of the stator core and windings of the prototype. The locations of the thermal resistors (Pt100) are: P1, P2 in end winding; P3-P5, P9 on stator end surface; P6-P8 on end winding surface.

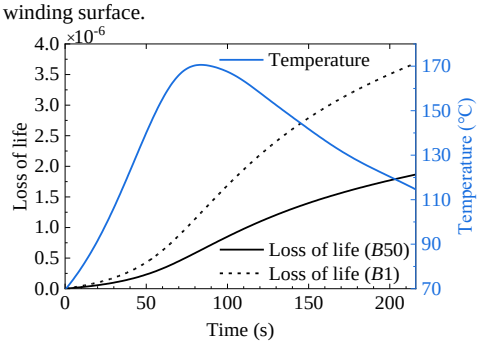

Fig. 17. The trends of loss of life over the temperature curve corresponding to the EMA mission.

TABLE VII

PREDICTED NUMBER OF CYCLES TO FAILURE AND TOTAL LIFETIME

Lifetime percentile	Number of cycles	Lifetime (Variable duty)	Lifetime (Continuous duty)
*B*1	$2.713\cdot10^5$	$1.636\cdot10^4$ h	$9.963\cdot10^3$ h
*B*50/MTTF	$5.360\cdot10^5$	$3.230\cdot10^4$ h	$2.044\cdot10^4$ h

VII. CONCLUSION

This paper presented a reliability-oriented multi-objective optimization approach of the low-voltage random-wound electrical machines as an attempt to cope with the design conflict between power density and reliability. This method is achieved by replacing the traditional empirical-based safety factor with a model-based reliability assessment (i.e., insulation thermal lifetime prediction) which is integrated as an optimization goal in a possible multi-objective optimization procedure. The proposed approach focuses on the thermal degradation of mainwall insulation and turn insulation of electrical machines, which are representative of the stator insulation system. Accelerated thermal degradation tests are carried out to build the thermal degradation model of insulation, combining the Wiener process with the Arrhenius equation. Based on the outcomes of the thermal degradation model, i.e., lifetimes, single-stress lifetime models are consequently built for both continuous duty and variable duty applications at required reliability levels (or lifetime percentiles) and employed as quantitative reliability assessment tools. A feasible reliability-oriented multi-objective optimization platform is built, based on which a realistic example implemented in aerospace application is addressed. The applicability of proposed reliability-oriented methodology is validated by the prototype. To the author knowledge, it is the first time that the reliability-oriented design methodology is fulfilled and employed in the design and optimization of low-voltage random-wound PMSM for aerospace application.

REFERENCES

[1] M. Galea, P. Giangrande, V. Madonna and G. Buticchi, "Reliability-Oriented Design of Electrical Machines: The Design Process for Machines' Insulation Systems MUST Evolve," *IEEE Ind. Electron. Mag.*, vol. 14, no. 1, pp. 20-28, March 2020.

[2] M. Galea. "High performance, direct drive machines for aerospace applications," Ph.D. dissertation, Department of Electrical and Electronic Engineering., Nottingham University, Nottingham, UK, 2013.

[3] K. T. Chau, C. C. Chan and C. Liu, "Overview of Permanent-Magnet Brushless Drives for Electric and Hybrid Electric Vehicles," *IEEE Trans. Ind. Electron.*, vol. 55, no. 6, pp. 2246-2257, June 2008.

[4] G. Pellegrino, A. Vagati, B. Boazzo and P. Guglielmi, "Comparison of Induction and PM Synchronous Motor Drives for EV Application Including Design Examples," *IEEE Trans. Ind. Appl.*, vol. 48, no. 6, pp. 2322-2332, Nov.-Dec. 2012

[5] S. F. Zhao, X. Y. Huang, Y. T. Fang and J. Li, "A control scheme for a High Speed Railway traction system based on high power PMSM," 2015 6th International Conference on Power Electronics Systems and Applications (PESA), 2015, pp. 1-8.

[6] Y. T. Fang and H. Zhang, "China's High-Speed Rail Technology: An International Perspective," Singapore: Springer, 2018.

[7] National Academies of Sciences, Engineering, and Medicine and others, Commercial aircraft propulsion and energy systems research: reducing global carbon emissions. National Academies Press, 2016.

[8] C. Dong, Y. Qian, Y. Zhang and W. Zhuge, "A Review of Thermal Designs for Improving Power Density in Electrical Machines," *IEEE Trans. Transport. Electrific.*, vol. 6, no. 4, pp. 1386-1400, Dec. 2020

[9] P. Wheeler, T. S. Sirimanna, S. Bozhko and K. S. Haran, "Electric/Hybrid-Electric Aircraft Propulsion Systems," in *Proceedings of the IEEE*, vol. 109, no. 6, pp. 1115-1127, June 2021.

[10] Z. Huang and J. Fang, "Multiphysics Design and Optimization of High-Speed Permanent-Magnet Electrical Machines for Air Blower Applications," *IEEE Trans. Ind. Electron.*, vol. 63, no. 5, pp. 2766-2774, May 2016.

[11] W. Zhao, X. Wang, C. Gerada, H. Zhang, C. Liu and Y. Wang, "Multi-Physics and Multi-Objective Optimization of a High Speed PMSM for High Performance Applications," *IEEE Trans. Magn.*, vol. 54, no. 11, pp. 1-5, Nov. 2018.

[12] A. Al-Timimy *et al.*, "Design and Losses Analysis of a High Power Density Machine for Flooded Pump Applications," *IEEE Trans. Ind. Appl.*, vol. 54, no. 4, pp. 3260-3270, July-Aug. 2018.

[13] X. Zhang and K. S. Haran, "High-specific-power electric machines for electrified transportation applications-technology options," *Proc. IEEE Energy Convers. Congr. Expo. (ECCE)*, 2016, pp. 1-8.

[14] V. Madonna, P. Giangrande, L. Lusuardi, A. Cavallini, C. Gerada and M. Galea, "Thermal Overload and Insulation Aging of Short Duty Cycle, Aerospace Motors," *IEEE Trans. Ind. Electron.*, vol. 67, no. 4, pp. 2618-2629, April 2020.

[15] T. W. Dakin, "Electrical Insulation Deterioration Treated as a Chemical Rate Phenomenon," *Trans. Amer. Inst. Electr. Eng.*, vol. 67, no. 1, pp. 113-122, Jan. 1948.

[16] E. A. Avallone, T. Baumeister and A. Sadegh, Marks' Standard Handbook for Mechanical Engineers, New York: McGraw-Hill, 2006.

[17] P. Zhang, Y. Du, and etc., "A Survey of Condition Monitoring and Protection Methods for Medium-Voltage Induction Motors," *IEEE Trans. Ind. Appl.*, vol. 47, no. 1, pp. 34-46, Jan.-Feb. 2011.

[18] W.B. Nelson. Accelerated Testing: Statistical Models, Test Plans, and Data Analysis. Wiley, New York, NY, USA, 2009.

[19] P. Giangrande, V. Madonna, S. Nuzzo and M. Galea, "Moving Toward a Reliability-Oriented Design Approach of Low-Voltage Electrical Machines by Including Insulation Thermal Aging Considerations," *IEEE Trans. Transport. Electrific.*, vol. 6, no. 1, pp. 16-27, March 2020.

[20] G. Lei, G. Bramerdorfer, B. Ma, Y. Guo and J. Zhu, "Robust Design Optimization of Electrical Machines: Multi-Objective Approach," *IEEE Trans. Energy Convers.*, vol. 36, no. 1, pp. 390-401, March 2021.

[21] B. Moore, R. Rehder, and R. Draper, "Utilizing reduced build concepts in the development of insulation systems for large motors," in *Proc. Electr. Insul. Conf. Electr. Manuf. Coil Winding Conf.*, Jan. 2003, pp. 347–352.

[22] V. Madonna, P. Giangrande and M. Galea, "Introducing Physics of Failure Considerations in the Electrical Machines Design," in *Proc. IEEE Int. Electric Mach. Drives Conf.* (*IEMDC*), San Diego, CA, USA, 2019, pp. 2233-2238

[23] *Evaluation and qualification of electrical insulation systems*, Standard IEC 60505:2011, IEC, 2011.

[24] Kunsong Lin, Yunxia Chen, Dan Xu, "Reliability assessment model considering heterogeneous population in a multiple stresses accelerated test," *Reliab. Eng. Syst. Safety.*, vol. 165, pp. 134-143, 2017.

[25] Xuerong Ye, Yifan Hu, Bokai Zheng, Cen Chen, Guofu Zhai, "A new class of multi-stress acceleration models with interaction effects and its extension to accelerated degradation modelling," *Reliab. Eng. Syst. Safety.*, vol. 228, 2022.

[26] *Rotating Electrical Machines - Part 18-41: Partial Discharge Free Electrical Insulation Systems (Type I) used in Rotating Electrical Machines Fed from Voltage Converters - Qualification and Quality Control Test*s, Standard IEC 60034-18-41: 2014, IEC, 2014.

[27] V. Madonna, P. Giangrande, W. Zhao, H. Zhang, C. Gerada and M. Galea, "Electrical Machines for the More Electric Aircraft: Partial Discharges Investigation," *IEEE Trans. Ind. Appl.*, vol. 57, no. 2, pp. 1389-1398, March-April 2021.

[28] Ji Y, Giangrande P, Madonna V, Zhao W, Galea M. "Reliability-Oriented Design of Inverter-Fed Low-Voltage Electrical Machines: Potential Solutions," *Energies*. 2021; 14(14):4144.

[29] L. Lusuardi, A. Cavallini, M. G. de la Calle, J. M. Martı́nez-Tarifa and G. Robles, "Insulation design of low voltage electrical motors fed by PWM inverters," *IEEE Electr. Insul. Mag.*, vol. 35, no. 3, pp. 7-15, May-June 2019.

[30] G. C. Stone, I. Culbert, E. A. Boulter and H. Dhirani, Electrical Insulation for Rotating Machines: Design, Evaluation, Aging, Testing and Repair, Hoboken, NJ, USA:Wiley, pp. 430-432, 2014.

[31] Z. Pang, X. Si, and et. al., "A Bayesian Inference for Remaining Useful Life Estimation by Fusing Accelerated Degradation Data and Condition Monitoring Data," *Reliab. Eng. Syst. Safety.*, vol. 208, Apr. 2021.

[32] H. Li, D. Pan and C. L. P. Chen, "Reliability Modeling and Life Estimation Using an Expectation Maximization Based Wiener Degradation Model for Momentum Wheels," *IEEE Trans. Cybern.*, vol. 45, no. 5, pp. 969-977, May 2015.

[33] *IEEE Standard Test Procedure for Thermal Evaluation of Systems of Insulating Materials for Random-Wound AC Electric Machinery*, IEEE Std 117-2015 (Revision of IEEE Std 117-1974), vol., no., pp.1-34, 6 May 2016.

[34] *Electric strength of insulating materials - Test methods - Part 2: Additional requirements for tests using direct voltage*, IEC 60243-2:2013, IEC, 2013.

[35] V. Madonna, P. Giangrande, G. Migliazza, G. Buticchi and M. Galea, "A Time-Saving Approach for the Thermal Lifetime Evaluation of Low-Voltage Electrical Machines," *IEEE Trans. Ind. Electron.*, vol. 67, no. 11, pp. 9195-9205, Nov. 2020.

[36] Y. S. Sherif and M. L. Smith, "First-Passage Time Distribution of Brownian Motion as a Reliability Model," *IEEE Trans. Reliab.*, vol. R-29, no. 5, pp. 425-426, Dec. 1980.

[37] Charles E. Ebeling. An Introduction to Reliability and Maintainability Engineering, McGraw-Hill, 1997.

[38] *Rotating electrical machines - Part 1: Rating and performance*, Standard IEC 60034-1:2022, IEC, 2022.

[39] *IEEE Recommended Practice for Insulation Testing of AC Electric Machinery with High Voltage at Very Low Frequency*, IEEE Std 433-2009 (Revision of IEEE Std 433-1974), vol., no., pp.1-30, 24 Feb. 2010.

[40] *IEEE Simplified Method for Calculation of the Regression Line (Appendix to IEEE Guide for the Statistical Analysis of Thermal Life Test Data*, IEEE Std 101-1972), IEEE Std 101A-1974, vol., no., pp.1-4, 12 Jan. 1974.

[41] Miner, M. A. "Cumulative Damage in Fatigue." *ASME. J. Appl. Mech*., 12(3), pp.159–164, Sept., 1945.

[42] *IEEE Recommended Practice for Measurement of Power Factor Tip-Up of Electric Machinery Stator Coil Insulation*, IEEE Std 286-2000, vol., no., pp.1-29, 1 March 2000.

[43] Y. Ji et al., "Partial Discharge Investigation Under Humidity Conditions via Dissipation Factor and Insulation Capacitance Tip-Up Test," *IEEE Trans. Dielectr. Electr. Insul.*, vol. 29, no. 4, pp. 1483-1490, Aug. 2022.

[44] H. Sedding, G. Stone and A. Shaikh, "Dielectric dissipation factor acceptance criteria for stator winding insulation," in *Proc. IEEE Int. Conf. Dielectr. (ICD)*, 2016, pp. 955-958.

[45] Y. Tian, R. Cheng, and et. al., "PlatEMO: A MATLAB Platform for Evolutionary Multi-Objective Optimization [Educational Forum]," *IEEE Comput. Intell. Mag.*, vol. 12, no. 4, pp. 73-87, Nov. 2017.

[46] C. Sciascera, P. Giangrande, L. Papini, C. Gerada and M. Galea, "Analytical Thermal Model for Fast Stator Winding Temperature Prediction," *IEEE Trans. Ind. Electron.*, vol. 64, no. 8, pp. 6116-6126, Aug. 2017

[47] K. Deb, A. Pratap, S. Agarwal and T. Meyarivan, "A fast and elitist multiobjective genetic algorithm: NSGA-II," *IEEE Trans. Evol. Comput.*, vol. 6, no. 2, pp. 182-197, April 2002.

[48] Y. Jin, H. Wang and C. Sun, Data-Driven Evolutionary Optimization: Integrating Evolutionary Computation, Machine Learning and Data Science, Switzerland: Springer, 2021.

[49] P. -D. Pfister, C. Tang and Y. Fang, "A Multi-Objective Finite-Element Method Optimization That Reduces Computation Resources Through Subdomain Model Assistance, for Surface-Mounted Permanent-Magnet Machines Used in Motion Systems," *IEEE Access*, vol. 11, pp. 8609-8621, 2023.